"Magic" orientation angles to suppress spin-driven Hall currents in anisotropic 2D materials with an ideal skyrmion gas

Andrei Zadorozhnyi and Yuri Dahnovsky*

Department of Physics and Astronomy/3905

1000 E. University Avenue

University of Wyoming

Laramie, WY 82071

E-mail: yurid@uwyo.edu

Abstract

The Hall effect depending on conduction electron spin projection becomes very different for anisotropic 2D crystals. In this case the spin-dependent electron current strongly determined by the orientation angle, θ, of the sample with respect to an applied electric field. The spin-up and -down components of the direct and Hall charge currents oscillate with the angle 2θ. The direct and Hall components of the current have the structure where there are the angle-independent part, oscillation amplitude, and phase shift. All three quantitates strongly depend on the electron spin projection, electron mass ratio, and skyrmion size. We find that there are "magic" orientation angles where the spin-up, spin-down, and total Hall currents vanish. There is a great interest in computations based on 2D materials with skyrmions. Such properties can be useful for computer logic operations based on skyrmions.

Introduction

Today studying the foundations of quantum mechanics has turned into a dynamic field initially linked to the explosive rise of quantum information theory. There is a fundamental minimum quantity of energy dissipated by a logic gate, in which information-carrying signals are continuously created and destroyed.[1] Reversible computing aims to circumvent this limitation by conserving information - and therefore energy - as signals propagate through a logic circuit.[2] In this scheme, conservative logical operations are executed through dissipation-free elastic interactions among these information carriers that conserve momentum and energy.[2] In a reversible skyrmion logic system skyrmions are conserved as they flow through nanowire tracks. Logical operations are performed by thoroughly leveraging the rich physics of magnetic skyrmions – the spin Hall effect[3] and the skyrmion Hall effect.[4–10] The interaction of skyrmions with free electrons can be one of the mechanisms that provide a device stability to the dissipation because of the topological integral of motion. Thus, within this paradigm it is important to study the dynamic properties of conduction electrons interacting with spin textures, skyrmions, where the topological state is conserved. In particular, we study an anomalous spin Hall effect of conduction electrons scattered by skyrmions in anisotropic 2D materials.

The mechanism of a spin-driven Hall effect is different than that of a charge Hall effect where a free electron deviates from its straight line trajectory due to the presence of a magnetic field or non-zero magnetic moments. The spin-driven Hall effect (SDHE) appears due to interaction of the conduction electrons with localized magnetic moment textures, skyrmions.[13–27] The schematic pictures for a skyrmion and electronic device is shown in Fig. 1. The skyrmions are very specific spin arrangements with distinct topological properties characterized by topological charges.[13,22,28–32]

In the previous investigations the mechanism of the conduction electrons scattering in an ideal skyrmion gas resulted in the dramatic charge currents dependencies on the concentration and spin projection of the conduction electrons and also on the skyrmion sizes. In

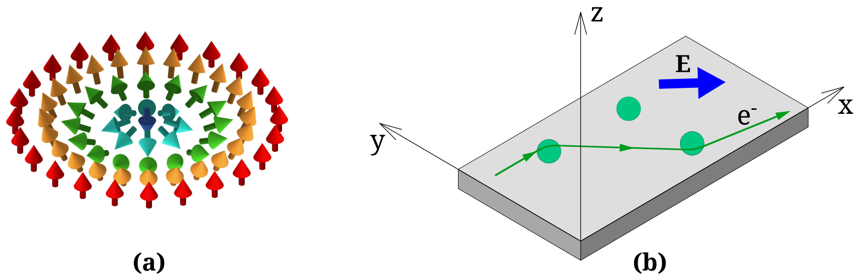

Figure 1: Schematic representations of (a) a skyrmion with the topological charge $Q = 1$ and (b) the electronic device made of an anisotropic 2D material. The green spots represent the skyrmions.

particular, spin-filtering and spin separation in the direction perpendicular to the electric field were found.[27] In addition, thermoelectric devices can exhibit the abrupt voltage switching in the spin Seebeck and Nernst effects.[33] For the calculations of spin currents in the x- and y-directions, we considered an isotropic material where the conduction electrons were presented as an ideal electron gas with an isotropic effective mass. The calculations were performed by using the Boltzmann equation where the electron scattering mechanism is due to the interaction of the electron spins with skyrmions' magnetic moments. The semiclassical approach based on the nonequilibrium Boltzmann equation[13,34–44] allowed us to find the spin currents in the whole range of the adiabaticity parameter. The polar symmetry for both skyrmions and the electron gas significantly simplified both numerical solutions of the Lippmann-Schwinger equation for the transition matrix and the Boltzmann equation for the nonequilibrium distribution function. In that case, the direction of the electric field was irrelevant.[27]

However, the orientation of a 2D anisotropic crystal can significantly change conduction electron scattering properties revealing new unusual effects depending on the orientation angle. In this work we assume that the skyrmions still have the polar symmetry, while the electron gas is anisotropic, i.e., the effective masses in x- and y-directions are different, as schematically shown in Fig. 2.

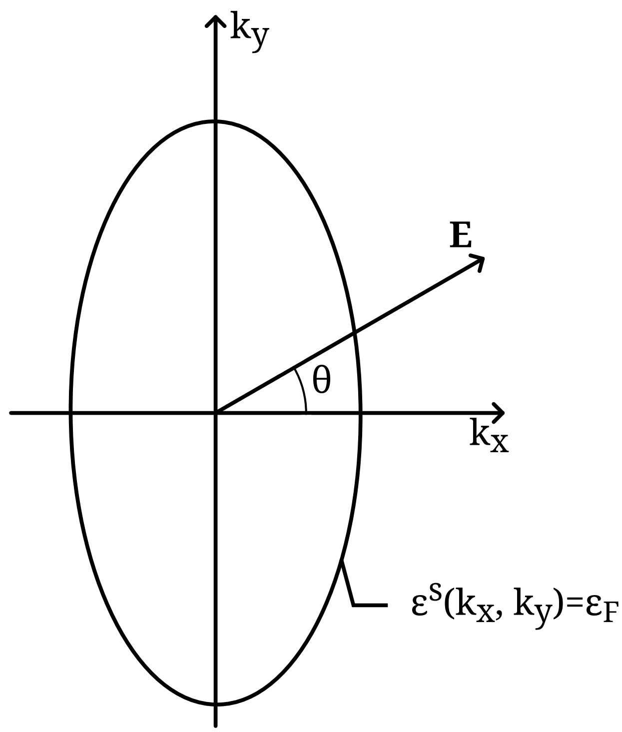

Figure 2: Orientation of the energy ellipse, $\varepsilon = \varepsilon^s(k_x, k_y)$ for conduction electrons, with respect to the applied electric field. The x- and y-axis coincide with the k_x and k_y directions, respectively.

Methods

To describe the conduction electron scattering by the skyrmions, we use the following $s-d$ Hamiltonian:[45]

$$H = \frac{\hbar^2 k_x^2}{2m_x} + \frac{\hbar^2 k_y^2}{2m_y} - J\mathbf{S}(\mathbf{r}) \cdot \boldsymbol{\sigma}, \tag{1}$$

where the first and second terms represent the kinetic energy of conduction electrons, J is an exchange integral, $\mathbf{S(r)}$ is a localized magnetic moment texture. Here $\boldsymbol{\sigma}$ is a vector with the three Pauli matrix projections for the conduction electron spins. The crystal anisotropy has been introduced by the different effective masses m_x, m_y, where it is assumed that $m_y > m_x$. We also choose the $\mathbf{S}(\mathbf{r})$-texture as follows:

$$\mathbf{S}(\mathbf{r}) = S_0 \cdot \mathbf{e}_z + \sum_i \delta\mathbf{S}(\mathbf{r} - \mathbf{r_i}). \tag{2}$$

Here, S_0 is uniform out-of-plane background magnetization and $\delta\mathbf{S}(\mathbf{r} - \mathbf{r_i})$ is a deviation of magnetic moment due to the presence of the skyrmions. The skyrmions (the topological charge $Q = 1$) are described by the following analytic equation $\delta\boldsymbol{S}(\boldsymbol{r}) = S_0\boldsymbol{n}(\boldsymbol{r})$, where

$$\begin{aligned} n_z(r) &= \left[\begin{array}{c} 4\left(\frac{2r}{d}\right)^2 - 2,\ r \leq d/4, \\ -4\left(1 - \frac{2r}{d}\right)^2,\ d/4 < r \leq d/2, \\ 0,\ r > d/2, \end{array} \right. \\ n_x(\boldsymbol{r}) &= \sqrt{1 - (n_z(r) + 1)^2} \cos\alpha, \\ n_y(\boldsymbol{r}) &= \sqrt{1 - (n_z(r) + 1)^2} \sin\alpha. \end{aligned} \tag{3}$$

In Eq. (3) d is the diameter of the skyrmion, r and α are polar coordinates with the center of the skyrmion located at $r = 0$.

To determine spin-dependent current densities parallel and perpendicular to the electric field $\boldsymbol{E}$, we employ the Boltzmann equation to find the nonequilibrium distribution functions:[46]

$$\frac{\partial f_0}{\partial \varepsilon}\boldsymbol{F}\cdot\boldsymbol{v}^s = \sum_{s'}\sum_{\boldsymbol{k}'}\left(W^{ss'}_{\boldsymbol{k}\boldsymbol{k}'} f_1^{s'}(\boldsymbol{k}') - W^{s's}_{\boldsymbol{k}'\boldsymbol{k}} f_1^{s}(\boldsymbol{k})\right), \tag{4}$$

where $W^{ss'}_{\boldsymbol{k}\boldsymbol{k}'}$ is a transition probability from the state with wavevector $\boldsymbol{k}'$ and spin s' to the state with wavevector $\boldsymbol{k}$ and spin s. f_0 is the equilibrium Fermi distribution function and f_1 is the first order correction to the distribution function. $\boldsymbol{F}$ is a force acting on the electron, and $\boldsymbol{v}$ stands for an electron velocity. The transition probability can be calculated in terms of transition matrix $T^{ss'}_{\mathbf{k}\mathbf{k}'}$:[47]

$$W^{ss'}_{\boldsymbol{k}\boldsymbol{k}'} = \frac{2\pi}{\hbar} n_t \left|T^{ss'}_{\boldsymbol{k}\boldsymbol{k}'}\right|^2 \delta(\varepsilon - \varepsilon'), \tag{5}$$

where n_t is the density of scatterers. The transition matrix can be found from the following Lippmann-Schwinger equation:[47]

$$\hat{T} = \hat{V} + \hat{V}\hat{G}_0\hat{T}, \tag{6}$$

where $\hat{G}_0$ is a retarded free electron Green's function determined in the following way:

$$\hat{G}_0(\varepsilon) = \lim_{\delta\to+0}\left[\varepsilon - \frac{k_x^2}{2m_x} - \frac{k_y^2}{2m_y} + J\boldsymbol{S}_0\cdot\hat{\boldsymbol{\sigma}} + i\delta\right]^{-1}, \tag{7}$$

and V is the potential energy for a single spin texture, which is given by the matrix:

$$\hat{V}(\mathbf{r}) = -J\begin{pmatrix} S_z & S_x - iS_y \\ S_x + iS_y & -S_z \end{pmatrix}. \tag{8}$$

To solve Lippmann-Schwinger (6) and Boltzmann equations (4), we have written the original code. $\hat{V}$-operator has been considered in a k-space, where the wavefunctions have been chosen to be the ordinary plane waves. The retarded Green's function has been calculated numerically. Lippman-Schwinger equation (6) has been solved in all orders of the interaction (see Eq. (8)) using the piecewise-constant approximation. In order to accelerate the calculations, we have used the H-adaptive mesh approach. The higher density mesh has been selected in the vicinity of the $\hat{G}_0$ singularities (see Eq. (7)). The lower density mesh has been employed for the grid cells located far away from the singularity curve. The nonequilibrium distribution function is a 2-element column, which dimension has been determined by the spin projections. As soon as the T-matrix is known and W rates are found, the solution of the Boltzmann equation (4) includes the inversion of the Boltzmann equation matrix. The complexity of the solution is due to the integral part of the collision integral in the k-space where the integrand contains the very narrow function close to the δ-function. This difficulty has been overcome by performing the additional integration of both left and right parts of the equation in the k-space in the vicinity of the curve determined by the delta function.

The current in the x- and y-directions has been calculated using the following equation:[46]

$$j_\alpha^s = \frac{e}{(2\pi)^2} \int v_\alpha f_1^s(\mathbf{k}) dk_x dk_y, \tag{9}$$

where $\alpha = x, y$.

Contrary to isotropic 2D materials, the orientation of an anisotropic crystal with respect to an applied electric field becomes important. The schematic picture of the orientation geometry is shown in Fig. 2. We have found that the angle dependences for the electric current can be described by the following equation (see Appendix):

$$\begin{aligned} j_\parallel^s(\theta) &= j_{0\parallel}^s + j_2^s \cos(2\theta + \varphi^s) \\ j_\perp^s(\theta) &= j_{0\perp}^s - j_2^s \sin(2\theta + \varphi^s) \end{aligned} \tag{10}$$

In this equation, $j_\parallel^s$ is the current component along with the direction of the applied electric field, $j_\perp^s$ is the Hall component of the electric current (the projection perpendicular to the electric field). The electric current has the angle-independent parts: $j_{0\parallel}^s$, $j_{0\perp}^s$, and the amplitudes in front of the *cos* and *sin* functions denoted as j_2^s. Eq. (10) contains the phase shift, φ^s, as well. Because of the time inversion symmetry, $\varepsilon(\boldsymbol{k}) = \varepsilon(-\boldsymbol{k})$, the angular dependence is 2θ instead of θ.

Eq. (10) has several remarkable properties: (a) the amplitudes for the parallel and the perpendicular components of the current are the same; (b) the parallel projection is described by the *cos*-function, while the perpendicular component is determined by the $-sin$-function; and (c) the phases for the perpendicular and parallel components are also the same. The proof of these properties is given in Appendix. In addition, there are two other important properties: (d) the Eq. (10) is valid for any $\varepsilon^s(\boldsymbol{k})$ (not only an ellipse) and (e) s can denote spin projections, energy band index, and valley index (see the proof in Appendix). Eq. (10) is valid for any scattering mechanism.

Results and discussion

The computations reveal some very interesting features in the electric current for parallel and perpendicular to the electric field components with spin-up and spin-down for the skyrmion size of 3.1 nm (such small skyrmions were predicted and observed in Pd/Fe/Ir materials)[11,12] and the different mass ratios as shown in Fig. 3. The curves in Fig. 3 completely satisfy to Eq. (10) for both direct and Hall components of the current. In all figures we observe the increase of the oscillation amplitudes with respect to the mass ratio. However, there are significant differences in the angle-independent part of the current, j_0 and the phase shifts. For example, for the parallel current the amplitude of the oscillation never exceeds the value of $j_{0\|}$. For the Hall current we find the zero value of the current for spin-down for some "magic" orientation angles. This property is useful in suppression of the Hall effect. This property can be used for logic devices in quantum computers.

The angular-independent parts of spin-up, spin-down current components are presented if Fig. 4. The skyrmion size is 3.1 nm. The parallel components of electric current for spin-up and spin-down exhibit the similar growing behavior with a slight difference (see Fig. 4a). $j^{\uparrow}_{0\|}.j^{\downarrow}_{0\|}$ for all values of mass ratio. However, the Hall component of j_0 (Fig. 4b) is

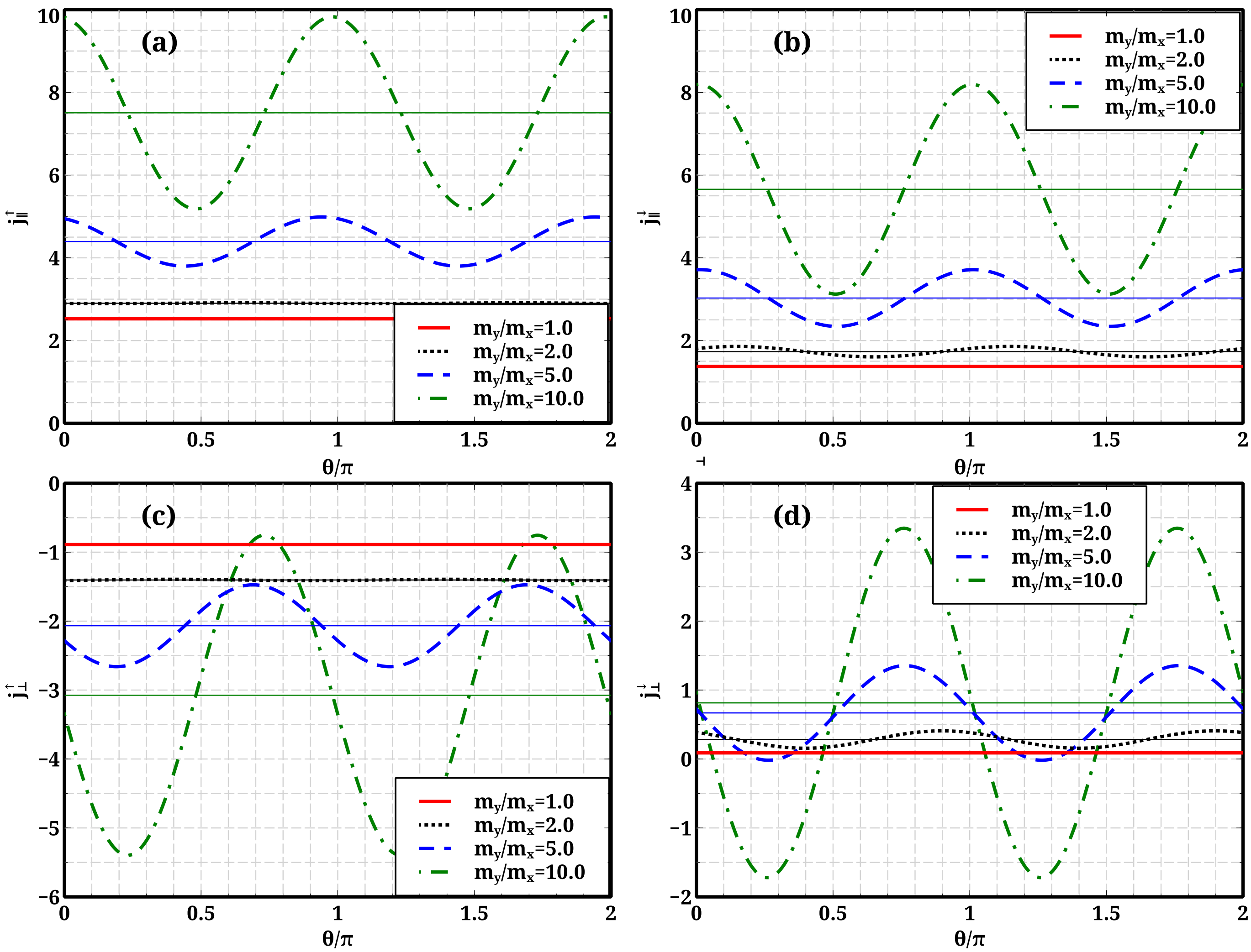

Figure 3: Orientation angle dependent currents for the skyrmion size $d = 3.1\ nm$,[11] and the various mass ratios $m_y/m_x = 1$, $m_y/m_x = 2$, $m_y/m_x = 5$, $m_y/m_x = 10$: (a) $j_{\parallel}^{\uparrow}$ is the current along with the electric field with spin-up carriers. (b) $j_{\parallel}^{\downarrow}$ is the current along with the electric field but with spin-down carriers, (c) $j_{\perp}^{\uparrow}$ is the Hall current (perpendicular to the electric field) with spin-up carriers, and (d) $j_{\perp}^{\downarrow}$ is the Hall current (perpendicular to the electric field) with spin-down carriers.

different: the absolute values of these components are the growing functions, but the signs of the amplitudes are different, $j_{0\perp}^{\uparrow} < 0$ and $j_{0\perp}^{\downarrow} > 0$.

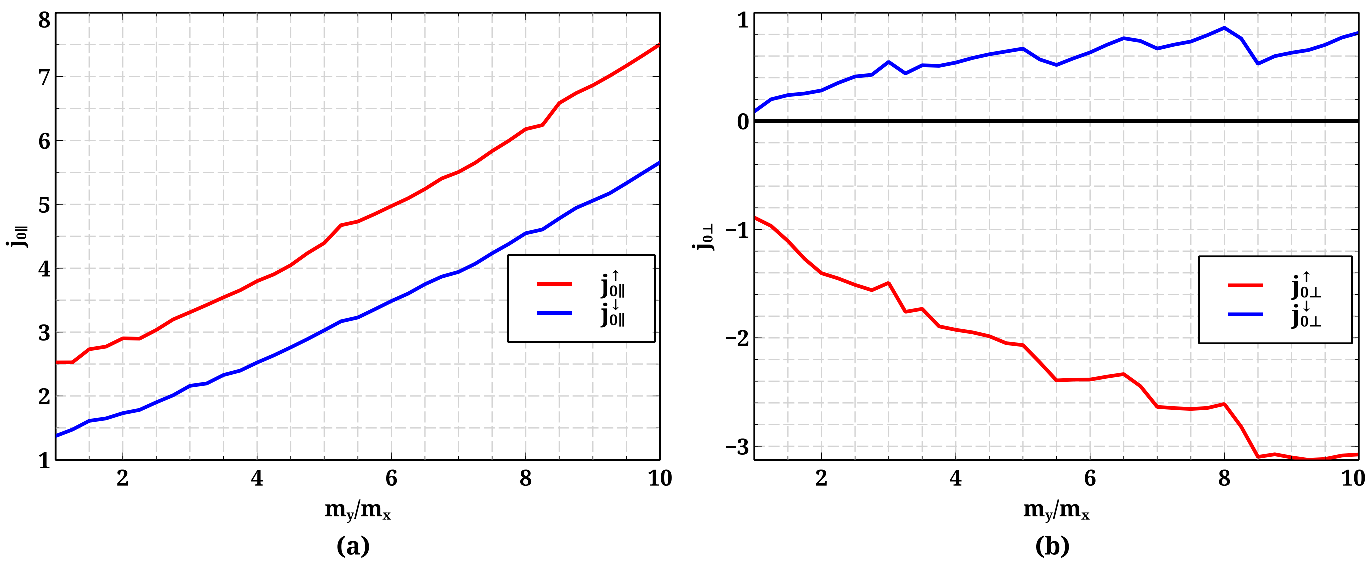

Figure 4: Zeroth order harmonics for the various mass ratios m_y/m_x with the skyrmion size of 3.1 nm, (a) component parallel to the electric field, and (b) perpendicular to the electric field (the Hall component of the current)

As follows from Eq. (10), the amplitude for the parallel and perpendicular components of the current are equal to each other. However, the spin-dependence still takes place. As shown if Fig. (5), $j_2^{\downarrow} > j_2^{\uparrow}$. $j_2^{\uparrow,\downarrow}$ are growing functions with the mass ratio. The skyrmion size is the same as in Fig. 4.

According to Eq. (10), the phases of the direct and Hall currents are the same. However, the spin dependence still takes place as shown in Fig. 6. For both spin-up and spin-down charge currents, the mass dependence are the nonlinear functions. In the spin-up case there is the strong peak at $m_y/m_x = 2$, and for spin-down there is the minimum at $m_y/m_x = 2$. For the higher mass ratios ($m_y/m_x > 4$), the phase converges to zero.

At some orientation angles and for some specific values of mass ratio it is possible to supress the Hall current for the spin-down, $j_{\perp}^{\downarrow}$ and total Hall currents $j_{\perp}^{\uparrow} + j_{\perp}^{\downarrow}$. Such angles are defined as the "magic" angles, $\theta_M^{\downarrow}$ and $\theta_M^{\uparrow+\downarrow}$, respectively. The mass ratio dependencies of "magic" angles are shown in Fig. 7. Interestingly, the "magic" angles do not exist in

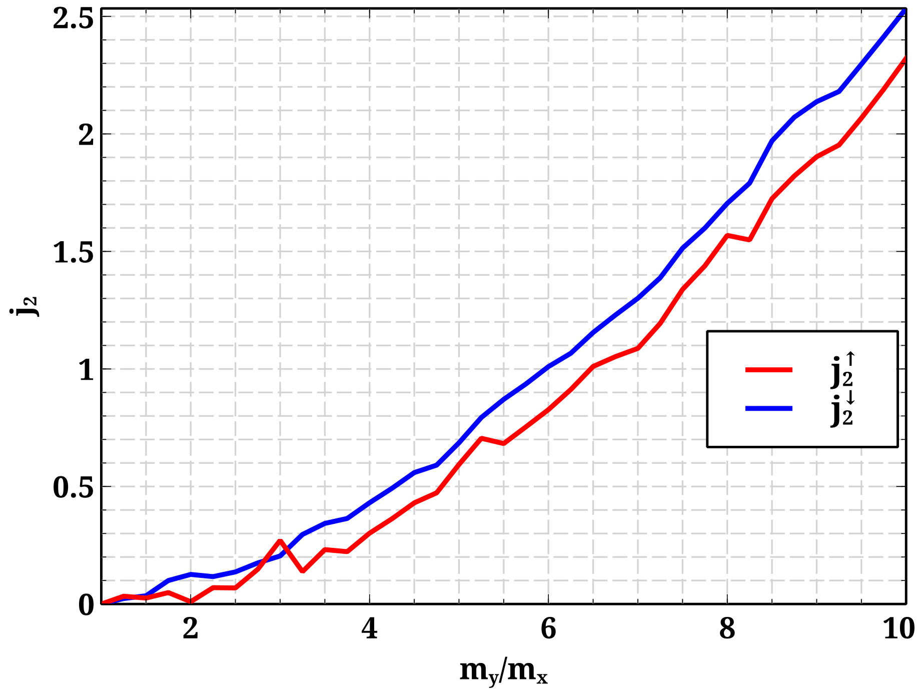

Figure 5: Second harmonics amplitude for both parallel and perpendicular components of the charge currents for the various mass ratios m_y/m_x with the skyrmion size of 3.1 nm.

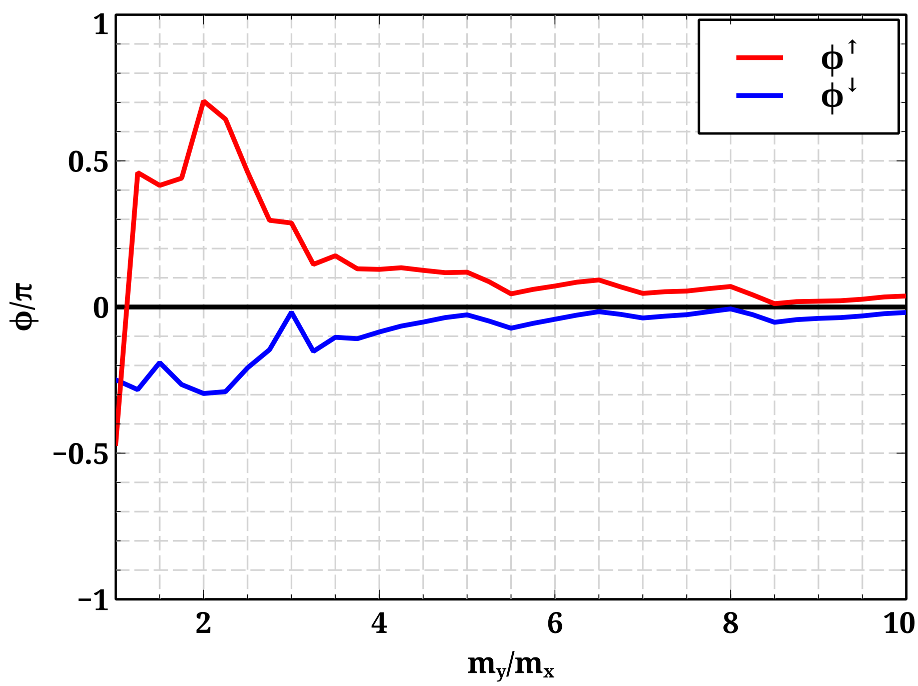

Figure 6: Phase shift for both direct and Hall components of the electric current for the various mass ratios m_y/m_x with the skyrmion size of 3.1 nm.

the whole range of the mass ratios. The threshold values for $\theta_M^{\downarrow}$ is $m_y/m_x = 5.0$, and for $\theta_M^{\uparrow+\downarrow}$ is $m_y/m_x = 6.0$. The "magic" angle does not exist for $j_{\perp}^{\uparrow}$ but it still take place for the sum because of opposite signs of $j_{0\perp}^{\downarrow}$ and $j_{0\perp}^{\downarrow}$ in this region. The orientation angle can be easily realized experimentally by changing the angle between an electric field and a sample. The orientation angles where the Hall current vanishes are very important for quantum computing.[7–10]

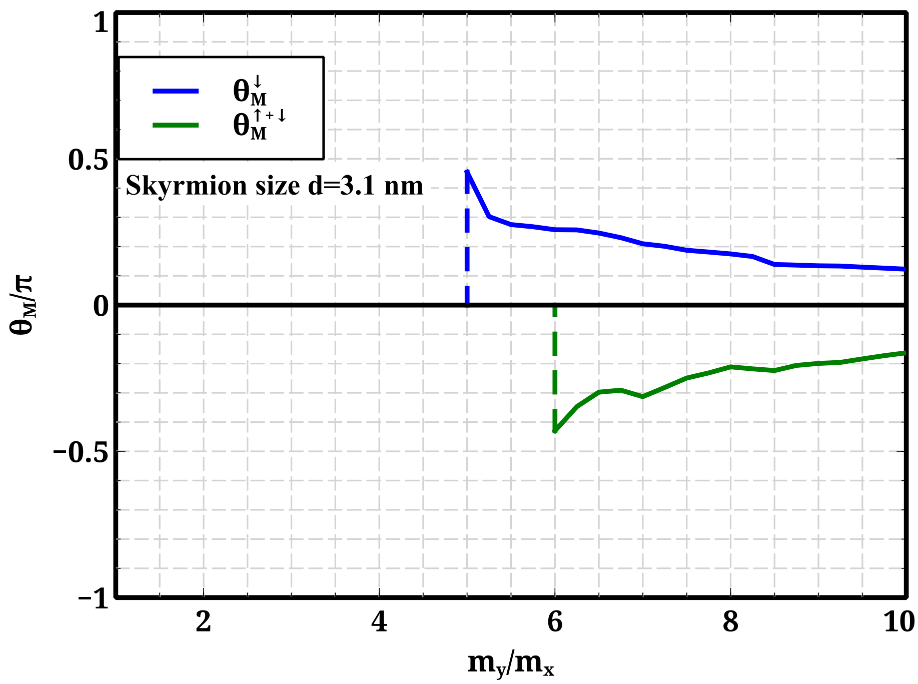

Figure 7: "Magic angles" for spin-down and for the sum of spin-up + spin-down components of the Hall currents for the various mass ratios m_y/m_x where the skyrmion size is chosen to be 3.1 nm.

Our next investigation is focused on the dependence of the electric current on skyrmion sizes with the fixed mass ratio, in our case $m_y/m_x = 3.0$. The angular-independent parts of the spin-up, spin-down current components significantly drop to the small values for the larger skyrmion sizes (see Fig. 8). The spin-down Hall current is always lower than that of the spin-up. For the larger skyrmion sizes, the more efficient scattering takes place because more localized spins from the skyrmion are involved into the scattering process.

As shown in Fig. 8b, the Hall current, however, exhibits the more dramatic behavior for the smaller skyrmions ($d \simeq 2$ nm). Both $j_{0\perp}^{\uparrow}$ and $j_{0\perp}^{\downarrow}$ are the negative growing functions.

For the larger skyrmions, the spin-up component drops again and further exhibits some oscillations remaining negative. The spin-down Hall current keeps growing and then becomes positive demonstrating some oscillations. For the very large sermon sizes, both components reach the plateaus as shown in Fig. 8b.

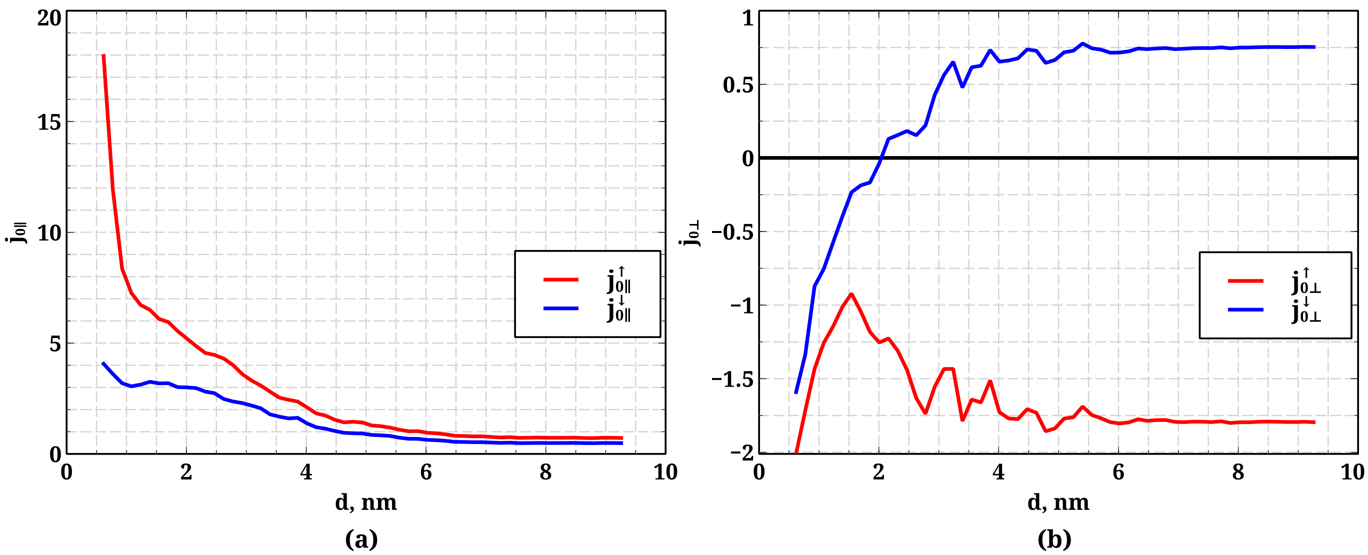

Figure 8: Zeroth order harmonic amplitudes for the different skyrmion sizes with the mass ratio of $m_y/m_x = 3.0$. (a) the current component parallel to the electric field and (b) the current component perpendicular to the electric field (the Hall current).

The amplitudes of the second harmonics for the spin-up and spin-down direct and Hall currents are shown in Fig. 9. The skyrmion size dependencies for both currents are very close to each other. They exhibit the minima and maxima at $d \approx 1$ nm and $d = 1.5$ nm, respectively.

The phases, ϕ, of the spin-up and spin-down currents for the various skyrmion sizes are presented in Fig. 10. The dependences exhibit highly nonlinear with some oscillations. The sharp minima at $d \approx 3.5$ nm and $d \approx 5.4$ nm with the broader maxima in the 3 $nm < d < 5$ nm region take place. For the large skyrmions ($d > 7$ nm) both phases drop to zero.

Furthermore, we study the "magic" angles where the spin-up, spin-down, and total Hall currents vanish. The spin-up Hall electric current is zero only at the singe skyrmion size, $d = 0.6$ nm and the orientation angle, $\theta^{\uparrow}_{M} \approx 0.2\pi$. The "magic" angles for the spin-down

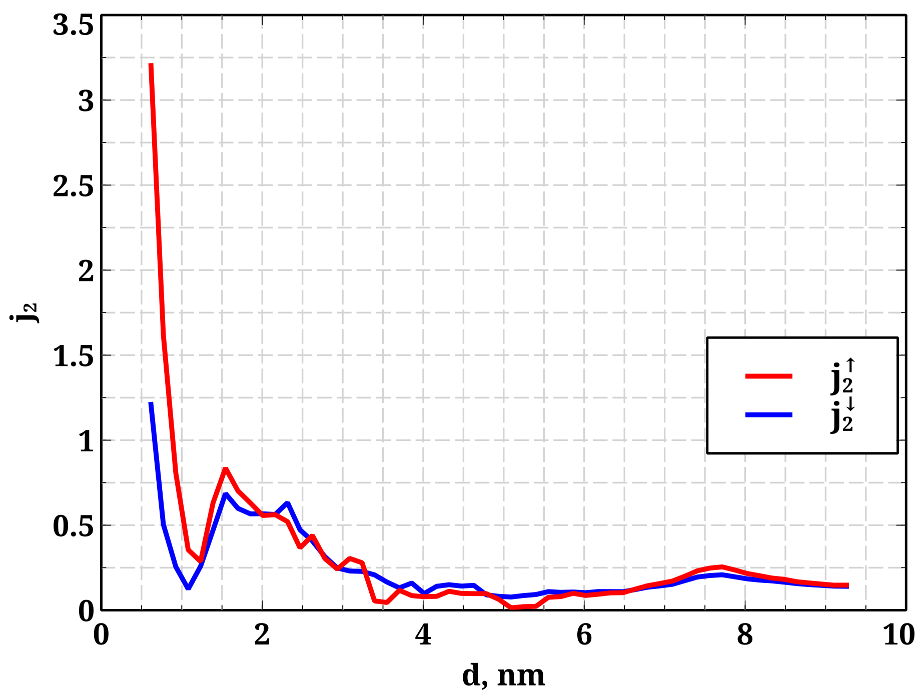

Figure 9: Second harmonics amplitude dependencies for both up- and down-spin projections with the skyrmion sizes. The mass ratio of $m_y/m_x = 3.0$.

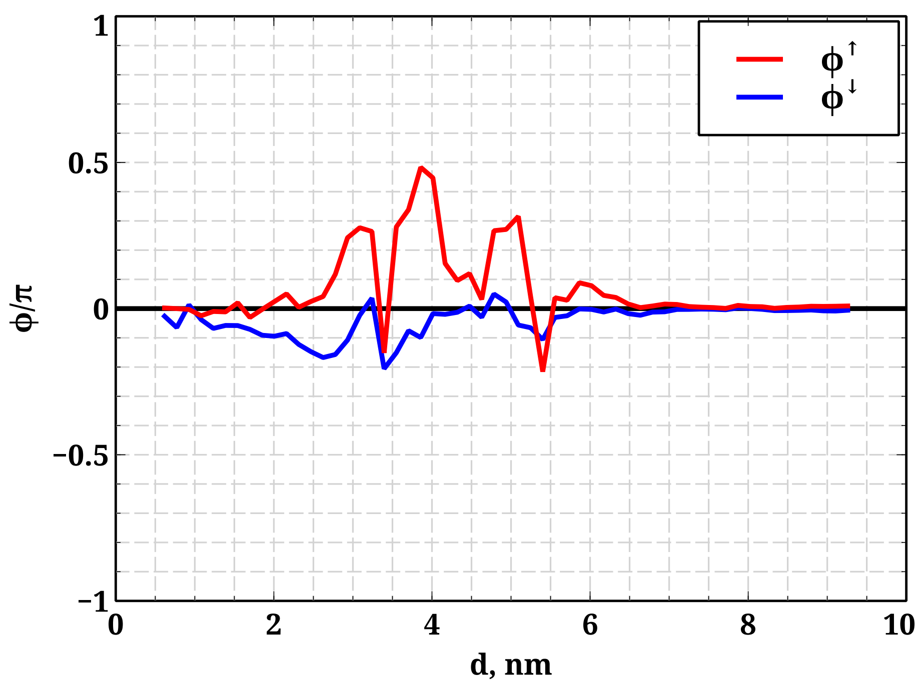

Figure 10: Phase shifts for both spin-up and spin-down electric current components with respect to the skyrmion sizes with the mass ratio of $m_y/m_x = 3.0$.

Hall current are presented by the whole curve with the two threshold values, $d = 1.4\ nm$ and $d = 2.8\ nm$ as shown in Fig. 11. For the sizes beyond this region there is no current. The "magic" angles for the total Hall current are depicted by the green crosses in Fig. 11. From the calculations we see that these dots do not make a continuous curve. We have found that the "magic" angles are always negative for the total Hall current.

The "magic" angles are very important for quantum computing in skyrmions because they can stabilize the skyrmion motion.[7–10]

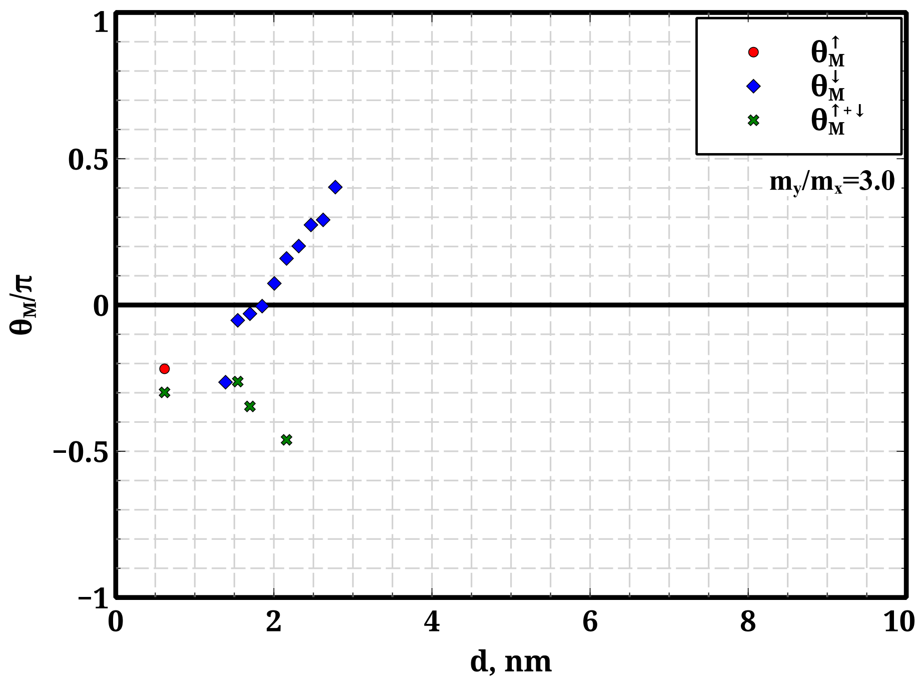

Figure 11: "Magic angles" for the spin-up, spin-down, and for the sum of spin-up and spin-down Hall currents for the various skyrmion sizes with the mass ratio of $m_y/m_x = 3.0$.

For all numerical calculations, we have assumed that $m_x = m_e$, while m_y is subjected to the change. The exchange integral ,J, in Eq. (1) is equal to $J = 0.4\ eV$. The Fermi energy is chosen to be $\varepsilon_F = 1\ eV$.

Conclusions

In this research we have studied the spin-dependent direct and Hall electric currents where the electrons are scattered by the spin textures (skyrmions) in anisotropic 2D crystals. Because the effective masses of the electrons in x- and y-directions are not equal to each other, the direct and Hall components strongly depend on the orientation angle of the crystal (see Fig. 2). We have found that the direct and Hall spin-up and spin-down electric currents are determined by the orientation angle θ in accordance with Eq. (10). This equation is valid for any $\varepsilon(\boldsymbol{k})$ (not only an ellipse), and the index s can denote spin projections, energy band, and valley number indexes (see Appendix.). In Eq. (10) a scattering mechanism is not specified. Thus, this equation is true for nay scattering process.

To find a spin-dependent electric current we have solved Boltzmann equation (4) where the transition matrices have been determined from Lippmann-Schwinger equation (6). The original code has been written for the solution of both Boltzmann and Lippmann-Schwinger equations. The Lippmann-Schwinger equation has been numerically solved in all orders with respect to the interaction between the conduction electrons and skyrmions (see Eq. (8)).

We have found that the Hall component of the electric current exhibits more dramatic behavior than the direct electric current. We have determined the dependencies of $j_{\parallel}^{\uparrow,\downarrow}$ and $j_{\perp}^{\uparrow,\downarrow}$ on the mass ratios and skyrmion sizes. These dependencies are very nonlinear.

For the stability of computers based on skyrmions, it is important to have vanishing Hall currents. Such currents can be achieved for some specific orientation angles, the "magic" angles. As shown in Fig. 7 and Fig. 11, the "magic" angles for the spin-down and the total Hall currents exist in certain regions with the threshold values of the parameters for the lower and upper limits.

Acknowledgments

This work was supported by a grant from the U S National Science Foundation (No. DMR-1710512) and the U S Department of Energy (No. 1004389) to the University of Wyoming.

Appendix

The skyrmion-driven Hall effect in anisotropic 2D materials exhibits the remarkable property – the dependence of the direct and Hall currents on the orientation angle as presented by Eq. (10). As described by Eq. (10), the direct and Hall currents have the angle- dependencies as θ have the form of $\cos\left(2\theta+\varphi\right)$ and $-\sin\left(2\theta+\varphi\right)$ with the same amplitude but different angle-independent components. In this Appendix we prove Eq. (10).

In order to find the orientation angle dependence of the electric current, we introduce the two auxiliary nonequilibrium distribution functions f_{1x}^{s} and f_{1y}^{s}, which obey the following auxiliary Boltzmann equations:

$$\begin{aligned}\frac{\partial f_0\left(\varepsilon^s\left(\boldsymbol{k}\right)\right)}{\partial\varepsilon}eEv_x^s\left(\boldsymbol{k}\right) &= \sum_{s'}\sum_{\boldsymbol{k}'}\left(W_{\boldsymbol{k}\boldsymbol{k}'}^{ss'}f_{1x}^{s'}(\boldsymbol{k}')-W_{\boldsymbol{k}'\boldsymbol{k}}^{s's}f_{1x}^{s}(\boldsymbol{k})\right),\\ \frac{\partial f_0\left(\varepsilon^s\left(\boldsymbol{k}\right)\right)}{\partial\varepsilon}eEv_y^s\left(\boldsymbol{k}\right) &= \sum_{s'}\sum_{\boldsymbol{k}'}\left(W_{\boldsymbol{k}\boldsymbol{k}'}^{ss'}f_{1y}^{s'}(\boldsymbol{k}')-W_{\boldsymbol{k}'\boldsymbol{k}}^{s's}f_{1y}^{s}(\boldsymbol{k})\right),\end{aligned} \tag{A1}$$

where x, y are arbitrary chosen axes which are tied to the crystal structure (i. e., the crystal doesn't move with respect to them). It is important to stress that f_{1x}^{s} and f_{1y}^{s} are not the components of a vector, but a more convenient representation of f_1^s.

Then we can present the in-plane electric field in the following form:

$$\boldsymbol{E}=E\begin{pmatrix}\cos\theta\\ \sin\theta\end{pmatrix}, \tag{A2}$$

where θ is the angle between $\boldsymbol{E}$ and x-axis, as shown in Fig. 2. For small electric field in the linear approximation, the nonequilibrium part of the distribution function can be represented in terms of the two auxiliary distribution functions as follows:

$$f_1^s(\boldsymbol{k}) = f_{1x}^s(\boldsymbol{k})\cos\theta + f_{1y}^s(\boldsymbol{k})\sin\theta. \tag{A3}$$

Using this form of the distribution function, we can find currents in x- and y-directions:

$$j_x^s = 2a_{xx}^s\cos\theta + 2a_{xy}^s\sin\theta, \qquad j_y^s = 2a_{yx}^s\cos\theta + 2a_{yy}^s\sin\theta, \tag{A4}$$

where the coefficients a_{xx}, a_{xy}, a_{yx}, a_{yy} are defined in the following way:

$$\begin{aligned} a_{xx}^s &= \frac{1}{2}e\int v_x^s(\boldsymbol{k})\, f_{1x}^s(\boldsymbol{k})\,\mathrm{dk_x dk_y}, \qquad & a_{xy}^s &= \frac{1}{2}e\int v_x^s(\boldsymbol{k})\, f_{1y}^s(\boldsymbol{k})\,\mathrm{dk_x dk_y}, \\ a_{yx}^s &= \frac{1}{2}e\int v_y^s(\boldsymbol{k})\, f_{1x}^s(\boldsymbol{k})\,\mathrm{dk_x dk_y}, \qquad & a_{yy}^s &= \frac{1}{2}e\int v_y^s(\boldsymbol{k})\, f_{1y}^s(\boldsymbol{k})\,\mathrm{dk_x dk_y}. \end{aligned} \tag{A5}$$

The coefficients a_{xx}, a_{xy}, a_{yx}, a_{yy} are θ-independent. As soon as the coefficients are known, we find the direct and Hall currents, which are the projections of the total electric current $\boldsymbol{j}^s$ on the axis parallel and perpendicular to the electric field.

$$\begin{aligned} j_\parallel^s &= j_x^s\cos\theta + j_y^s\sin\theta = \left(a_{xx}^s + a_{yy}^s\right) + \left(a_{xx}^s - a_{yy}^s\right)\cos 2\theta + \left(a_{xy}^s + a_{yx}^s\right)\sin 2\theta, \\ j_\perp^s &= -j_x^s\sin\theta + j_y^s\cos\theta = \left(a_{yx}^s - a_{xy}^s\right) - \left(a_{xx}^s - a_{yy}^s\right)\sin 2\theta + \left(a_{xy}^s + a_{yx}^s\right)\cos 2\theta. \end{aligned} \tag{A6}$$

Performing some trigonometrical transformations and introducing the following definitions, we obtain

$$\begin{gathered} j_{0\parallel}^s = a_{xx}^s + a_{yy}^s, \quad j_{0\perp}^s = a_{yx}^s - a_{xy}^s, \quad j_2^s = \sqrt{\left(a_{xx}^s - a_{yy}^s\right)^2 + \left(a_{xy}^s + a_{yx}^s\right)^2}, \\ \sin\varphi^s = -\frac{a_{xy}^s + a_{yx}^s}{j_2^s}, \qquad \cos\varphi^s = \frac{a_{xx}^s - a_{yy}^s}{j_2^s}, \end{gathered} \tag{A7}$$

where Eq. (A6) transforms to the following form:

$$\begin{aligned} j_\parallel^s &= j_{0\parallel}^s + j_2^s\cos\left(2\theta + \varphi^s\right), \\ j_\perp^s &= j_{0\perp}^s - j_2^s\sin\left(2\theta + \varphi^s\right). \end{aligned} \tag{A8}$$

The derivations presented above are rather general and valid for any energy band form. In addition, we have not specified the mechanism of scattering. Therefore, the formulas derived are valid for any material and any scattering mechanisms. Index s is very general and can identified a spin projection, band number or valley number.

References

(1) Landauer R. Irreversibility and heat generation in the computing process. *IBM Journal of Research and Development* **1961**, *5*, 183-191.

(2) E. Fredkin E.; Toffoli, T. Conservative logic. *Int. Journ Theor. Phys.* **1982**, *21*, 219-253.

(3) Sinova, J; Valenzuela, S. O.; Wunderlich, j.; Back, C. H.; Jungwirth, T. Spin Hall effects. *Rev. Mod. Phys.* **2015**, *87*, 1213-1260.

(4) Jiang, W.; Zhang, X.; Yu, G.; Zhang, W.; Wang, X.; Jungfleisch, M. B.; Pearson, J. E.; Cheng, X.; Heinonen, O.; Wang, K. L. et al. Direct observation of the skyrmion Hall effect. *Nat. Phys.* **2017**, *13*, 162-169.

(5) Litzius, K.; Lemesh, I.; Kruger, B.; Bassirian, P.; Caretta, L.; Richter, K.; Buttner, F.; Sato, K.; Tretiakov, O. A.; Forster, J. et al. Skyrmion Hall effect revealed by direct time-resolved X-ray microscopy. *Nat. Phys.* **2017**, *13*, 170-175.

(6) Lin, S. Z.; Reichhardt, C.; Batista, C. D.; Saxena, A. Particle model for skyrmions in metallic chiral magnets: Dynamics, pinning, and creep. *Phys. Rev. B* **2013**, *87*, 214419.

(7) Purnama, I.; Gan, W. L.; Wong, D. W.; Lew, W. S. Guided current-induced skyrmion motion in 1D potential well. *Sci. Rep.* **2015**, *5*, 10620.

(8) Zhang, X.; Zhou, Y.; Ezawa, M.; Magnetic bilayer-skyrmions without skyrmion Hall effect. *Nat. Commun.* **2016**, *7*, 10293.

(9) Barker, J.; Tretiakov, O. A. Static and Dynamical Properties of Antiferromagnetic Skyrmions in the Presence of Applied Current and Temperature. *Phys. Rev. Lett.* **2016**, *116*, 147203.

(10) Zhang, X.; Zhou, Y.; Ezawa, M. Antiferromagnetic skyrmion: Stability, creation and manipulation. *Sci. Rep.* **2016**, *6*, 24795.

(11) X. S. Wang, X. S.; H. Y. Yuan,H. Y.; X. R. Wang, X. R. A theory on skyrmion size. *Commun. Phys.* **2018**, *1*, 31.

(12) Romming, N.; Hanneken, C.; Menzel, M.; Bickel, J. E.; Wolter, B.; von Bergmann, K.; Kubetzka, A.; Wiesendanger, R. Writing and Deleting Single Magnetic Skyrmions. *Science* **2013**, *341* , 636-639.

(13) Nagaosa, N.; Sinova, J.; Onoda, S.; MacDonald, A. H.; Ong, N. P. Anomalous Hall effect. *Rev. Mod. Phys.* **2010**, *82*, 1539-1592.

(14) Lee, M.; Kang, W.; Onose, Y.; Tokura, Y.; Ong N. P. Unusual Hall Effect Anomaly in MnSi under Pressure. *Phys. Rev. Lett.* **2009**, *102*, 186601.

(15) Neubauer, A.; Pfleiderer, C.; Binz, B.; Rosch, A.; Ritz, R.; Niklowitz, P. G.; Boni, P. Topological Hall Effect in the A Phase of MnSi. *Phys. Rev. Lett.* **2009**, *102*, 186602.

(16) Machida, Y.; Nakatsuji, S.; Maeno, Y.; Tayama T, Sakakibara, T.; Onoda, S. Unconventional Anomalous Hall Effect Enhanced by a Noncoplanar Spin Texture in the Frustrated Kondo Lattice $Pr_2Ir_2O_7$. *Phys. Rev. Lett.* **2007**, *98*, 057203.

(17) Surger, C.; Fischer, G.; Winkel, P.; Lohneysen, H. V. Large topological Hall effect in the non-collinear phase of an antiferromagnet. *Nat. Commun.* **2014**, *5*, 3400.

(18) Ueland, B. G.; Miclea, C. F.; Kato, Y.; Ayala–Valenzuela, O.; McDonald, R. D.; Okazaki, R.; Tobash, P. H.; Torrez, M. A.; Ronning, F.; Movshovich, R. et al. Controllable chirality-induced geometrical Hall effect in a frustrated highly correlated metal. *Nat. Commun.* **2012**, *3*, 1067.

(19) Fabris, F. W.; Pureur, P.; Schaf, J.; Vieira, V. N.; Campbell, I. A. Chiral anomalous Hall effect in reentrant AuFe alloys. *Phys. Rev. B* **2006**, *74*, 214201.

(20) Ohuchi, Y.; Kozuka, Y.; Uchida, M.; Ueno, K.; Tsukazaki, A.; Kawasaki, M. Topological Hall effect in thin films of the Heisenberg ferromagnet EuO. *Phys. Rev. B* **2015**, *91* (24), 245115

(21) Oveshnikov, L. N.; Kulbachinskii, V. A.; Davydov, A. B.; Aronzon, B. A.; Rozhansky, I. V.; Averkiev, N. S.; Kugel, K. I.; Tripathi, V. Berry phase mechanism of the anomalous Hall effect in a disordered two-dimensional magnetic semiconductor structure. *Sci. Rep* **2015**, *5*, 17158.

(22) Nagaosa, N.; Tokura, Y. Topological properties and dynamics of magnetic skyrmions. *Nat. Nanotechnol.* **2013**, *8*, 899-911.

(23) Kanazawa, N.; Kubota, M.; Tsukazaki, A.; Kozuka, Y.; Takahashi, K. S.; Kawasaki, M.; Ichikawa, M.; Kagawa, F.; Tokura Y. Discretized topological Hall effect emerging from skyrmions in constricted geometry. *Phys. Rev. B* **2015**, *91*, 041122(R).

(24) Muhlbauer, S.; Binz, B.; Jonietz, F.; Pfleiderer, C.; Rosch, A.; Neubauer, A.; Georgii, R.; Boni, P. Skyrmion lattice in a chiral magnet. *Science* **2009**, *323*, 915-919.

(25) Li, Y.; Kanazawa, N.; Yu, X. Z.; Tsukazaki, A.; Kawasaki, M.; Ichikawa, M.; Jin, X. F.; Kagawa, F.; Tokura, Y. Robust Formation of Skyrmions and Topological Hall Effect Anomaly in Epitaxial Thin Films of MnSi. *Phys. Rev. Lett.* **2013**, *110*, 117202

(26) Bruno, P.; Dugaev, V. K.; Taillefumier, M. Topological Hall Effect and Berry Phase in Magnetic Nanostructures. *Phys. Rev. Lett.* **2004**, *93*, 096806.

(27) Zadorozhnyi, A.; Dahnovsky, Y. Spin filtering and spin separation in 2D materials by topological spin Hall effect. *J. Phys.: Condens. Matter* **2020**, *32*, 405803.

(28) Onoda, M.; Tatara, G.; Nagaosa, N. Anomalous Hall Effect and Skyrmion Number in Real and Momentum Spaces. *J. Phys. Soc. Jpn* **2004**, *73*, 2624-2627.

(29) Tatara, G.; Kawamura, H. Chirality-Driven Anomalous Hall Effect in Weak Coupling Regime. *J. Phys. Soc. Jpn* **2002**, *71*, 2613-2616.

(30) Ohe, J.; Ohtsuki, T.; Kramer, B. Mesoscopic Hall effect driven by chiral spin order. *Phys. Rev. B* **2007**, *75*, 245313.

(31) Ndiaye, P. B.; Akosa, C. A,; Manchon, A. Topological Hall and spin Hall effects in disordered skyrmionic textures. *Phys. Rev. B* **2017**, *95*, 064426.

(32) Ye, J.;Kim, Y. B.; Millis, A. J.; Shraiman, B. I.; Majumdar, P.; Tesanovic, Z. Berry Phase Theory of the Anomalous Hall Effect: Application to Colossal Magnetoresistance Manganites. *Phys. Rev. Lett.* **1999**, *83*, 3737-3740.

(33) Zadorozhnyi, A.; Dahnovsky, Y. Spin-dependent Seebeck and Nernst effects in an ideal skyrmion gas. *J. Magn. Magn. Mater* **2021**, *518*, 167367.

(34) Luttinger, J. M.; Kohn, W. Motion of Electrons and Holes in Perturbed Periodic Fields. *Phys. Rev.* **1955**, *97*, 869-883.

(35) Luttinger, J. M. Theory of the Hall Effect in Ferromagnetic Substances. *Phys. Rev.* **1958**, *112*, 739-751.

(36) Smit, J. The spontaneous hall effect in ferromagnetics I. *Physica* **1955**, *21*, 877-887.

(37) Berger, L. Side-Jump Mechanism for the Hall Effect of Ferromagnets. *Phys. Rev. B* **1970**, *2* (11), 4559-4566.

(38) Jungwirth, T.; Niu, Q.; MacDonald, A. H. Anomalous Hall Effect in Ferromagnetic Semiconductors. *Phys. Rev. Lett.* **2002**, *88*, 207208.

(39) Sinitsyn, N. A. Semiclassical theories of the anomalous Hall effect. *J. Phys. Condens. Matter* **2007**, *20*, 023201.

(40) Sinitsyn, N. A.; MacDonald, A. H.; Jungwirth, T.; Dugaev, V. K.; Sinova, J. Anomalous Hall effect in a two-dimensional Dirac band: The link between the Kubo-Streda formula and the semiclassical Boltzmann equation approach. *Phys. Rev. B* **2007**, *75*, 045315.

(41) Sinitsyn, N. A.; Niu, Q.; MacDonald, A. H. Coordinate shift in the semiclassical Boltzmann equation and the anomalous Hall effect. *Phys. Rev. B*, 2006, *73*, 075318.

(42) Sinitsyn, N. A.; Niu, Q.; Sinova, J.; Nomura, K. Disorder effects in the anomalous Hall effect induced by Berry curvature. *Phys. Rev. B* **2005**, *72*, 045346.

(43) Denisov, K. S.; Rozhansky, I. V.; Averkiev, N. S.; Lahderanta, E. Electron Scattering on a Magnetic Skyrmion in the Nonadiabatic Approximation. *Phys. Rev. Lett.* **2016**, *117*, 027202.

(44) Denisov, K. S.; Rozhansky, I. V.; Averkiev, N. S.; Lahderanta, E. General theory of the topological Hall effect in systems with chiral spin textures. *Phys. Rev. B* **2018**, *98*, 195439.

(45) Hewson, A. C. *The Kondo Problem to Heavy Fermions*; Cambridge University Press: Cambridge, UK, 1993.

(46) Anselm, A. *Introduction to Semiconductor Theory*; Mir Moscow, USSR, 1981.

(47) Taylor, J. R. *Scattering Theory: The quantum Theory on Nonrelativistic Collisions*; Wiley: New York, USA, 1972.

(48) Tomasello, R.; Martinez, E.; Zivieri, R.; Torres, L.; Carpentieri, M.; Finocchio, G. A strategy for the design of skyrmion racetrack memories. *Scientific Reports* **2014**, *4*, 6784.